



CHORUS

This is the accepted manuscript made available via CHORUS. The article has been published as:

Competition between Polar and Nonpolar Lattice Distortions in Oxide Quantum Wells: New Critical Thickness at Polar Interfaces

J. Gazquez, M. Stengel, R. Mishra, M. Scigaj, M. Varela, M. A. Roldan, J. Fontcuberta, F. Sánchez, and G. Herranz

Phys. Rev. Lett. **119**, 106102 — Published 7 September 2017

DOI: [10.1103/PhysRevLett.119.106102](https://doi.org/10.1103/PhysRevLett.119.106102)

Competition between polar and nonpolar lattice distortions in oxide quantum wells: a new critical thickness at polar interfaces

J. Gazquez¹, M. Stengel^{1,2}, R. Mishra³, M. Scigaj¹, M. Varela^{4,5}, M.A. Roldan⁵, J. Fontcuberta¹, F. Sánchez¹, G. Herranz¹

¹Institut de Ciència de Materials de Barcelona, Campus de la UAB, 08193, Bellaterra, Spain

²ICREA, Pg. Lluís Companys 23, 08010 Barcelona, Spain.

³Department of Mechanical Engineering and Materials Science, Washington University in St. Louis, St. Louis, MO 63130, USA

⁴Materials Science and Technology Division, Oak Ridge National Laboratory, TN 37831-6071, USA

⁵Departamento de Física de Materiales & Instituto Pluridisciplinar, Universidad Complutense de Madrid. Madrid, 28040, Spain

Two basic lattice distortions permeate the structural phase diagram of oxide perovskites: antiferrodistortive (AFD) rotations and tilts of the oxygen octahedral network and polar ferroelectric modes. With some notable exceptions, these two order parameters rarely coexist in a bulk crystal, and understanding their competition is a lively area of active research. Here we demonstrate, by using LaAlO₃/SrTiO₃ system as a test case, that quantum confinement can be a viable tool to shift the balance between AFD and polar modes, and selectively stabilize one of the two phases. In particular, by combining scanning transmission electron microscopy and first-principles based models, we find a crossover between a bulk-like LaAlO₃ structure to a strongly polar state with no AFD tilts at a thickness of approximately three unit cells, therefore, in addition to the celebrated electronic reconstruction, our work unveils a second critical thickness, not related to the electronic properties, but to the structural ones. We discuss the implications of these findings, both for the specifics of the LaAlO₃/SrTiO₃ system, and for the general quest towards nanoscale control of materials properties.

Polar lattice distortions [1, 2] and "antiferrodistortive" (AFD) tilts of the BO_6 octahedral network [3,4] are ubiquitous in the physics of ABO_3 perovskite oxides, and largely responsible for their interesting functional properties. Indeed, the former, associated with an unstable zone-center optical phonon of the cubic reference structure, potentially leads to ferroelectricity, while the latter, mediated by a zone-boundary mode, often have a dramatic impact over the orbital and magnetic orders. Although some notable exceptions exist (e.g. $BiFeO_3$), the two order parameters tend to be mutually contraindicated in a bulk perovskite crystal [3]. Such a competition has often been used in the continuing search for new multiferroics, or more generally to engineer exotic phases via atomic-scale design, as in the recent report of polar metals at perovskite interfaces [5]. Overall, controlling the balance between the competing polar/AFD phases offers exciting opportunities to realize novel properties "à la carte". Such a balance is often delicate, as both types of lattice distortions and their mutual couplings are governed by a subtle interplay of short-range covalency (related to $B-O$ bonding) and long-range electrostatic (or elastic) effects [6].

Atomic-scale confinement appears as an ideal tool to tune the competition between different order parameters, as it is known to profoundly alter the spectrum of lattice and electronic excitations of crystalline insulators [7–11]. In the context of ferroelectrics, for example, size effects play a dramatic role in determining the stability of the polar state [12,13]. Note that the main driving force that determines the critical thickness for ferroelectricity is of electrostatic nature, and manifests itself as a "depolarizing" electric field that is antiparallel to the polarization of the film. From this perspective, the question of whether nonferroelectric (and hence insensitive to macroscopic depolarizing effects) modes such as the AFD tilts may also experience a "critical thickness" emerges as a particularly interesting one. Apart from the academic interest, suppressing (or partially destabilizing) the AFD tilts may be also useful for practical applications. Manganites and nikelates are good examples where magnetic and transport properties are sensitive to the O–B–O bond angles bridging adjacent BO_6 octahedra, and, thus, prone to large changes induced by modulation of the AFD tilts [14].

The interface between $LaAlO_3$ and $SrTiO_3$ –two prominent compounds in the field of oxide electronics [15] – provides an excellent model system to address the effect of confinement on AFD and/or polar lattice distortions. On one hand, according to the "polar catastrophe model", the *electrostatic* mismatch at the $LaAlO_3/SrTiO_3$ interface produces a strong internal electric field in the $LaAlO_3$ layer at subthreshold thicknesses (less than 4 unit cells). Such field is neutralized at larger thicknesses via spontaneous electron transfer from the free surface to the interface Ti(3d) orbitals, hereby forming a high-mobility 2DEG [16–19]. Interestingly, the subthreshold electric field has been predicted [20,21] to strongly polarize the $LaAlO_3$ lattice, but a direct experimental confirmation is still missing. On the other hand, there is a *structural* mismatch at the interface as well: $LaAlO_3$, either in bulk or thin-film form, presents large AFD tilts at room temperature, while the $SrTiO_3$ substrate adopts an undistorted cubic phase at the same temperature and, therefore, their juxtaposition appears problematic if the continuity of the O network is to be preserved. Therefore, in ultrathin $LaAlO_3/SrTiO_3$ heterostructures we have the unique coexistence of an electrostatic and a structural frustration, which either individually or cooperatively may lead to emerging properties *within* the $LaAlO_3$ layer. As both confinement and electric fields can be controlled experimentally, they could be used, in principle, as a switch to toggle the ground state of the system between competing phases, as illustrated in Figure 1(a).

Here we used high-resolution annular bright-field (ABF) in scanning transmission electron microscopy (STEM) to map the positions of all ions (including O columns) across the $LaAlO_3/SrTiO_3$ interface, for a varying thickness t of the $LaAlO_3$ overlayer. We find that, for a subcritical ($t < 4$ unit cells) $LaAlO_3$ film, nonpolar AFD distortions are suppressed in favor of a strong polar distortion within the film. This result provides, at the same time, unambiguous evidence

in support of the "polar-catastrophe" model, and a direct demonstration of how the AFD modes can be controlled at the nanoscale. A numerical model based on first-principles density-functional theory (DFT) indicates that the spatial confinement within LaAlO_3 is indeed the driving force for the AFD suppression. Interestingly, our theoretical model also predicts a nonnegligible interaction (via a repulsive biquadratic term) between the polar modes and the AFD tilts; we find that the latter is important for achieving a quantitative agreement with the experimentally observed critical thickness. All in all, our work reveals that no less than three phase transitions occur simultaneously at a LaAlO_3 thickness of about three unit cells: a metal-insulator transition at the interface driven by the 2DEG formation, and two lattice transitions where the AFD modes disappear and a polar state emerges in their place.

Figures 1(b) and (c) show the Z -contrast (upper right panels) and ABF (upper left panels) images of 3 and 7 uc-thick LaAlO_3 layers, respectively. Images of a 5 uc-thick sample can be found in the Supplementary Information [22]. The magnified ABF images [lower panels of Fig. 1(b) and (c)] reveal, even to the naked eye, important variations of the LaAlO_3 structure as a function of its thickness. These structural changes were quantified using a center-of-mass refinement on the contrast-inverted ABF images to determine the atomic position. In these calculations, we verified that any bias introduced by the varying background signal close to the interface negligible, see the Supplementary Information [22] for further details. In this way, we could accurately determine the location of all the atomic sites along with the interface plane, indicated by the arrow in the image of Fig. 1(b). From the atomic positions, we could obtain a detailed real-space map of both polar and AFD modes within the LaAlO_3 film, which we shall describe in the following.

First, we extracted (Fig. 2(a-d)) the polar shifts (δ_B, δ_O), whereby the B and O sub-lattices are off-centered with respect to the A sublattice. In the 3 uc-thick LaAlO_3 layer both δ_B, δ_O are *negative*, i.e. the Al and O atoms move towards the interface relative to the La sublattice. The fact that Al atoms also move downward may seem at first counterintuitive, however, as our model calculations predict – see supplementary Figure S10–, in the presence of an electric field the polar displacements are dominated by the upward movement of the La. Moreover, the measured Al and O shifts show excellent agreement with our first-principles calculations, and the corresponding non-zero relative displacement ($\delta_B > \delta_O$), which is the most relevant parameter, indicates a net electrical dipole pointing away from the substrate (Fig. 2(c)). This finding demonstrates the presence of polar distortions in LaAlO_3 , confirming prior theoretical predictions [20], and consistent with the presence of an internal field in subcritical LaAlO_3 layers, as predicted by the polar catastrophe scenario. To verify this point, we performed first-principles calculations of LaAlO_3 under the influence of a macroscopic electric displacement, D_z . After structural relaxation, we extracted δ_B and δ_O as a function of D_z (Figure S10). Remarkably, we find excellent agreement with the experimentally measured values for $D_z \sim 0.65 \times e/2a_0^2$ (a_0 is the in-plane lattice parameter), confirming the electrostatic nature of the observed distortions. The resulting internal field, although smaller than the expected value ($D_z = e/2a_0^2$) for the ideal insulating interface [17,18], provides unequivocal support to the so-called "polar catastrophe" model [16]. Indeed, our measured polar shifts in the 5-uc (see Supplementary Information [22]) and 7-uc samples gradually decrease to significantly smaller values (Fig. 2(d) and Fig. S3), as anticipated for above-threshold (and hence electrostatically compensated) films ($> 4\text{uc}$). Interestingly, polar distortions in SrTiO_3 near the interface are also visible; their behavior is overall in fair agreement with the first-principles predictions [21] and with earlier experimental observations [33,34]. Interestingly, our electron energy loss spectroscopy (EELS) analysis shows that the scale of the structural distortions present in the SrTiO_3 uppermost layers is larger than the interdiffusion length scale, which rules out any correlation between the observed distortions and the chemical interdiffusion across the interface.

Second, as sketched in Fig. 3(a), we isolated the tilting patterns of the BO_6 octahedral units by measuring the rippling within the visible portion of the O sublattice. Such rippling is due to the presence of octahedral tilts along $[100]_{pc}$ and $[010]_{pc}$ directions corresponding to the amplitude of the $[110]_{pc}$ -oriented antiferrodistortive (AFD) mode ($a^-a^-a^0$ pattern in Glazer notation), which we quantify via the projected rotation angle α . In both the 5 and the 7 uc-thick layers, the rotation angles are overall quite large near the film surface ($\alpha \approx 3.5 - 4^\circ$, Fig. 3(b)), and progressively decrease to zero when moving towards the SrTiO₃ substrate. Both the observation of an in-plane tilt axis and the measured distortion amplitude are consistent with the first-principles predictions of Hatt and Spaldin for a LaAlO₃ film under tensile strain [35]; also, a decrease of α towards the interface was expected -- recall that SrTiO₃ at room temperature has a cubic structure with no AFD tilts. In contrast, in the 3 uc-thick layer (Fig. 3(b)) the rotations are *completely* suppressed, except for the uppermost Al-O-Al plane, where $\alpha \approx 1.2^\circ$. Remarkably, such an abrupt suppression of the oxygen AFD tilts *occurs at the same critical thickness at which we observe a drastic increase in the polar distortions* (see Fig. 2(c)).

To shed some light on the observed evolution of the polar and antiferrodistortive degrees of freedom as a function of thickness, we considered a Landau-type energy functional that describes the energetics of the AFD modes and their interaction with electric fields,

$$F(\phi, D_z) = \frac{A}{2}\phi^2 + \frac{B}{4}\phi^4 + \frac{C}{2}\phi^2 D_z^2 + \frac{G}{2}\left(\frac{\partial\phi}{\partial z}\right)^2 \quad (\text{Equation 1})$$

Here ϕ is related to the amplitude of the in-plane AFD tilt and, thus, to the rotation angle α . The first two terms in Equation 1 encode the tendency of the crystal to distort spontaneously, where A is negative, and the positive quartic coefficient B guarantees the overall thermodynamic stability. The third term in Equation 1 describes the bi-quadratic repulsion between the AFD tilts and the internal electric field (described by the displacement D_z), well known in ferroelectric perovskites [36–38]. C is an "effective" biquadratic coefficient that implicitly includes the contribution of secondary lattice modes [39]. The fourth term in Equation 1 penalizes AFD mode gradients, which appear inevitably because at room temperature the AFD rotations must vanish at the boundary with SrTiO₃. Except for the gradient couplings, this model (and the computational approach to calculating the coefficients) is similar in spirit to that of Ref. [40].

The coefficients A , B , C and G in Equation 1 were extracted from a set of first-principles calculations, which we performed in the framework of the local density approximation (LDA) to density-functional theory (DFT) (a full description is reported in the Supplementary Information [22]). In particular, A and B were obtained by computing the energy difference between the undistorted lattice and the fully relaxed structure with optimized $a^-a^-a^0$ pattern; C was extracted from two sets of constrained- D calculations, performed either with or without relaxing the AFD tilts. In practice, an additional $\phi^2 D_z^4$ term was introduced in Equation 1 to improve the accuracy at large fields. The latter observation is substantiated by the data plotted in Fig. 3(c), which show that, at large fields, the inclusion of the additional quadratic-quartic $\phi^2 D_z^4$ term improves substantially the fitting of Equation 1 to the DFT data. Finally, the coefficient G was obtained by fitting the lowest unstable phonon branch of the undistorted cell along the RM path in reciprocal space (i.e., the ϕ_x, ϕ_y doublet corresponding to in-plane AFD tilts indicated by the dashed red curve in Fig. 3(d)). Interestingly, above a critical wavevector ($q_{crit} = 0.16$), the ϕ_x, ϕ_y phonon frequency becomes positive, which implies that at wavelength shorter than $1/q_{crit} \sim 6.5uc$ a spatially modulated AFD distortion cannot occur spontaneously. This observation embodies the essence of the confinement effects that we discuss in this work: an unstable lattice mode is eventually suppressed if the positive gradient energy becomes too strong.

After setting the boundary conditions that best reproduce the experimental observations (Figure 3(b) shows that the tilt amplitude in LaAlO₃ behaves qualitatively as air vibrations in an open-ended pipe, i.e. with a node at the interface and a maximum at the free surface), we initially solved our model *in the absence of an electric field*. We obtain a critical thickness for the emergence of AFD tilts of about 2 unit cells (Fig. 3(e)), which is significantly smaller than the experimental one. The key to solving this inconsistency resides in the effect of internal fields on the AFD modes. To demonstrate this important point, we used Equation 1 to estimate the field-induced change in the energy gain (ΔE_{AFD}) associated to the relaxation, and therefore the presence of the AFD tilts. The results (Fig. 3(c)) show a clear general trend, namely, internal fields significantly increase the critical thickness for the appearance of AFD tilts. For instance, distortions in the 2-uc system are suppressed when $D_z > 0.6 \times e/2a_0^2$. For the 3-uc layer a larger field $D_z \sim e/2a_0^2$ is required (Fig. 3(c)), roughly the expected value for the ideal electronic reconstruction [17,18]. Therefore, *both* internal fields and spatial confinement are necessary to explain the unexpected suppression of the tilts in the 3-uc LaAlO₃ film. This result, together with the direct observation of strong polar distortions, provide a strong case supporting the “polar catastrophe” model, which predicts the existence of such a field for insulating interfaces (< 4 uc), but its unambiguous detection has been so far elusive.

Summing up, our work reveals that the strong competition between octahedral tilts and polar displacements results in the emergence of two simultaneous reconstructions in the LaAlO₃/SrTiO₃ system (Fig. 1(a)). In particular, in addition to the celebrated metal-insulator transition, our results show that an extra reconstruction occurs on the LaAlO₃ side, driven by the action of an electric field on AFD modes. This indicates that controlling electric fields inside a lattice may provide an additional way to reversibly activate octahedral distortions in atomically confined perovskites, possibly enabling dynamic modulation of their functionalities. We explored this interesting possibility with an additional computational experiment in which we artificially neutralized the internal field within the LaAlO₃ film (Supplementary Information [22]). The results (Fig. 3(f)) show that the suppression of the internal field triggers the reemergence of the AFD distortions, consistent with the predictions of our continuum model. This test opens up enticing prospects. For instance, in the case of the LaAlO₃/SrTiO₃ system, the internal field may be manipulated by directly writing charges on the surface [41,42]. Similar approaches may be used to modulate magnetism [43] or ferroelectricity [44] in other systems, thus significantly expanding the scopes of materials design at perovskite interfaces. We conclude, therefore, that this kind of complex interplay may be used as a general tool to engineer potentially useful physical properties in atomically-thin ABO₃-perovskite structures.

Supplemental Material

The Supplementary Information contains the details of the Synthesis of $\text{LaAlO}_3/\text{SrTiO}_3$ heterostructures, also the electron microscopy data from the 5 uc-thick LaAlO_3 layer, together with the procedure for the structural parameters quantification and the theoretical calculations.

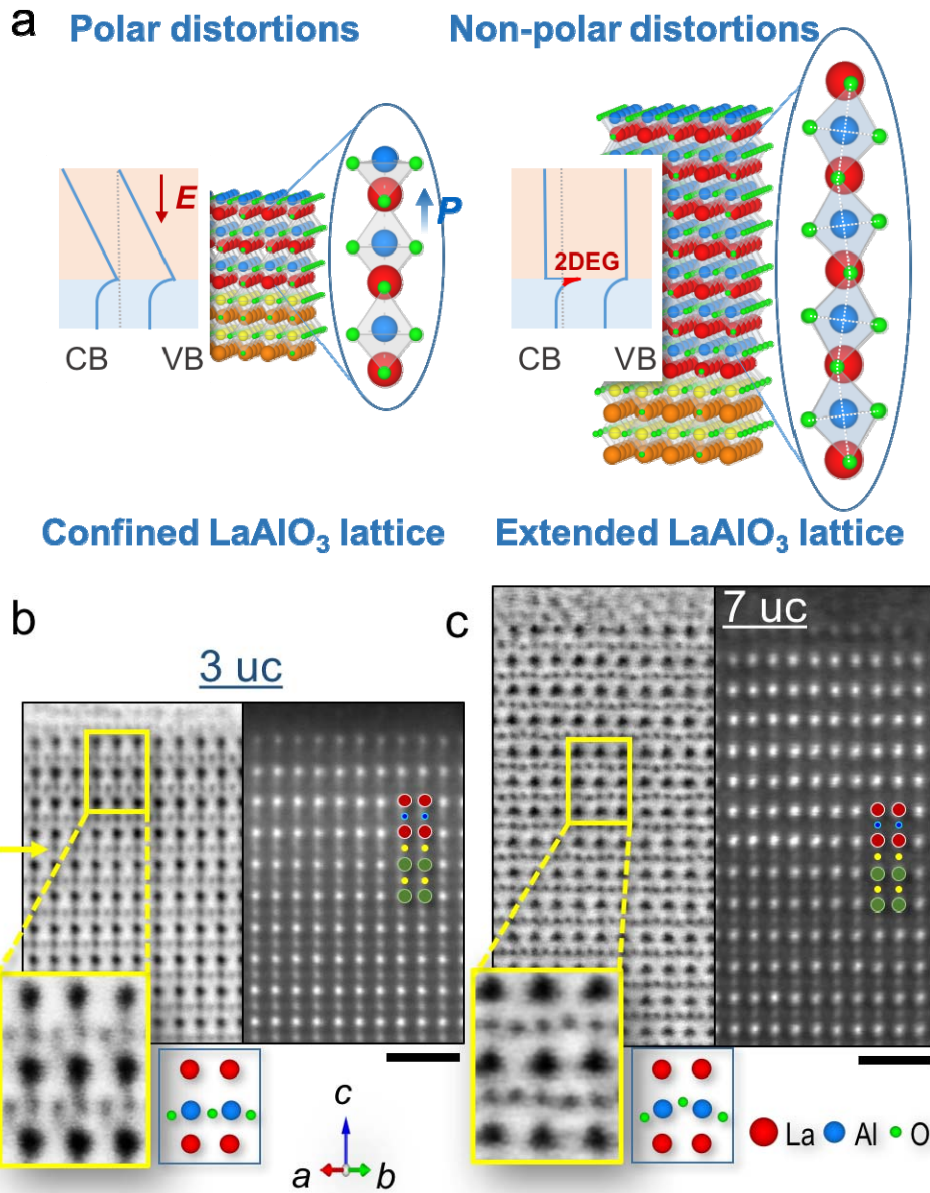


Figure 1 | (a) Polar and nonpolar antiferrodistortive (AFD) tilts in LaAlO₃ in LaAlO₃/SrTiO₃ heterostructures. Schematic structures of the polar displacements and octahedral tilts in LaAlO₃ film of thicknesses below and above the critical one for 2DEG formation in SrTiO₃: < 4 u.c. (left panel) and > 4 u.c. (right panel), respectively. (b-c) Atomic-scale mapping of the interface. Upper panel, b-c) Z-contrast (right) and ABF (left) simultaneously acquired STEM images of 3, and 7 uc-thick LaAlO₃/SrTiO₃ samples, respectively, viewed along the [110] zone axis. The [110] pseudocubic projection allows visualizing the buckling of the O sub-lattice. Lower panel, zoomed out regions of the ABF images of the 3, and 7 uc-thick LaAlO₃ layers along with schematics of the LaAlO₃ structure showing the distortions revealed by the ABF images, being La in red, Al in blue and O in green. Scale bar, 1 nm.

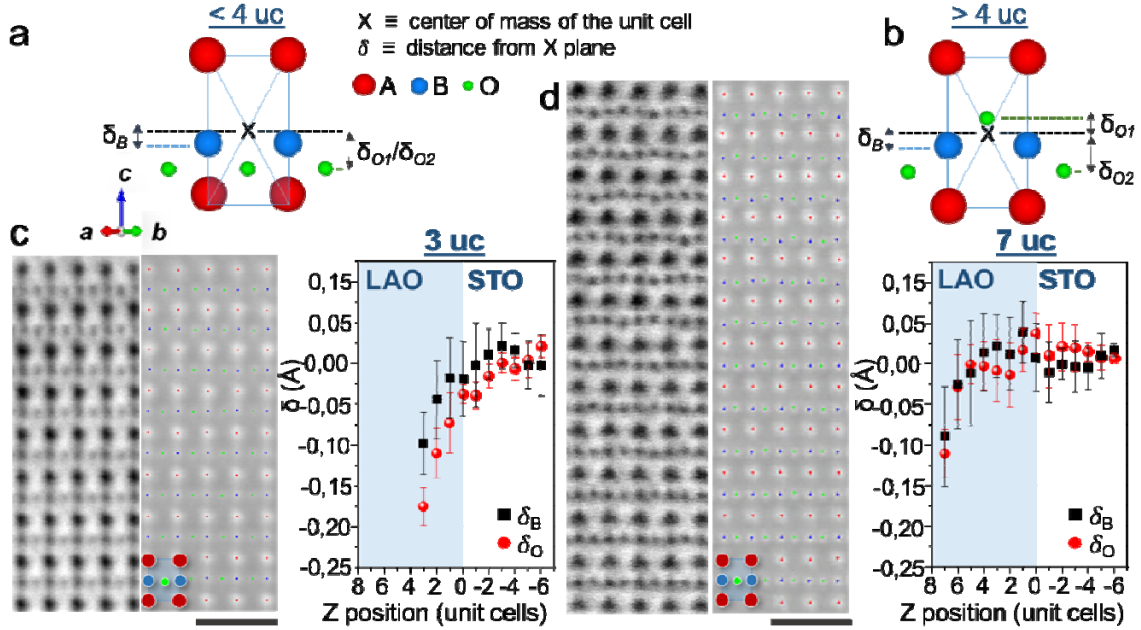


Figure 2] Quantitative analysis of polar shifts. a) and b), schematics of the distortions revealed by the ABF images shown in Figure 1. These adapted perovskite ABO_3 unit cells viewed along the $[110]$ zone axis show the distance δ from the center of mass of the unit cell (marked with a cross) and that of the B and $O1$ and $O2$ sites for a < 4 u.c. (a) and > 4 u.c. (b) thick $LaAlO_3$ layers. The schemes show the displacements of B and O atoms from the center of the unit cell. A , B and O atoms are shown in red, blue and green, respectively. The represented atomic displacements are not in scale. From left to right, c-d) show ABF and inverted ABF images along with the averaged values of the distance δ of the B (black squares) and O (red circles) sites from the center of mass of each unit cell (right panel) as a function of position of the 3, and 7 uc-thick samples, respectively. Scale bar, 1 nm.

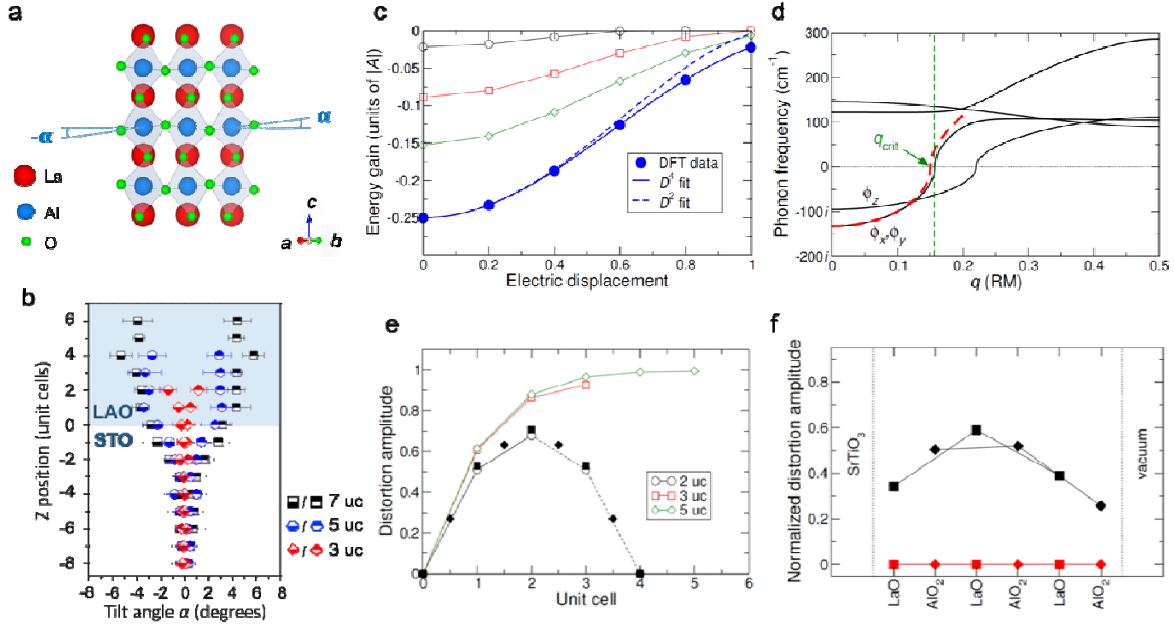


Figure 3 | Experimentally measured antiferrodistortive tilts and first-principles analysis. a) [110] view of the LaAlO_3 structure showing octahedral tilts. La, Al and O are shown in red, blue and green, respectively. b) $B-O-B$ tilt angle along the z -axis, as a function of thickness. The tilting of the 3, 5 and 7 uc-thick samples are shown in red, blue and black, respectively. The error bars show the standard deviation with respect to the average for each atomic layer. The light blue shade marks the LaAlO_3 layer. c) Energy per unit cell associated to the tilts as a function of the dielectric displacement, ϵ . The filled blue circles show the first-principles results for a uniform tilt pattern, calculated as the energy difference between a distorted and undistorted geometry. The solid and dashed blue curves are fits, respectively including or excluding the additional quadratic-quartic term. The empty symbols are model results for confined tilt patterns: Results for 2-uc (black circles), 3-uc (red squares) and 5-uc (green diamonds) films are shown. The electric displacement is in units of ϵ_0 . d) Phonon dispersion curves of the reference undistorted (but elastically strained) cell along the RM segment in the Brillouin zone. The dashed red curve shows a quadratic fit of the lowest unstable branch. e) Distortion amplitude as a function of film thickness (same color/symbol code as in panel B), as predicted by the model Eq. (1). The 2-uc film with asymmetric boundary conditions (solid line) is shown as an equivalent 5-uc segment with symmetrical blocking boundary conditions (dashed line). The filled symbols correspond to the amplitudes extracted from an explicit first-principles calculation (see Supplementary Information [22]). f) AFD distortions (black symbols) in a thin (3-uc thick) LaAlO_3 layer deposited on a SrTiO_3 substrate, with the internal field neutralized via external surface charges (see Supplementary Information for details [22]). In the “pristine” system (red symbols) the tilts as they are suppressed by the strong internal field.

Acknowledgements

This work was supported by the Spanish MAT2014-56063-C2-1-R, Severo Ochoa SEV-2015-0496 grant, the RyC-2012-11709 contract of J.G. and the Generalitat de Catalunya (2014 SGR 734) project. Electron microscopy observations at ORNL were supported by the U.S. Department of Energy (DOE), Basic Energy Sciences (BES), Materials Sciences and Engineering Division. M.S. acknowledges the support of MINECO through Grants MAT2016-77100-C2-2-P, FIS2013-48668-C2-2-P and of Generalitat de Catalunya (Grant No. 2014 SGR301). Calculations were performed at the Supercomputing Center of Galicia (CESGA). The authors are also grateful to Nico Dix for his collaboration in the growth of the films. Research at UCM sponsored by Fundación BBVA and Spanish MINECO MAT2015-66888-C3-3-R.

References

- [1] R. E. Cohen, *Nature* **358**, 136 (1992).
- [2] K. M. Rabe, C. H. Ahn, J. M.-M. Triscone, M. Dawber, and C. Lichtensteiger, *Physics of Ferroelectrics* (2007).
- [3] U. Aschauer and N. A. Spaldin, *J. Phys. Condens. Matter* **26**, 122203 (2014).
- [4] J. M. Rondinelli and C. J. Fennie, *Adv. Mater.* **24**, 1961 (2012).
- [5] T. H. Kim, D. Puggioni, Y. Yuan, L. Xie, H. Zhou, N. Campbell, P. J. Ryan, Y. Choi, J.-W. Kim, J. R. Patzner, S. Ryu, J. P. Podkaminer, J. Irwin, Y. Ma, C. J. Fennie, M. S. Rzchowski, X. Q. Pan, V. Gopalan, J. M. Rondinelli, and C. B. Eom, *Nature* **533**, 68 (2016).
- [6] P. Aguado-Puente, P. García-Fernández, and J. Junquera, *Phys. Rev. Lett.* **107**, 217601 (2011).
- [7] A. A. Balandin and D. L. Nika, *Mater. Today* **15**, 266 (2012).
- [8] M. Maldovan, *Nature* **503**, 209 (2013).
- [9] N. Li, J. Ren, L. Wang, G. Zhang, P. Hänggi, and B. Li, *Rev. Mod. Phys.* **84**, 1045 (2012).
- [10] J. Hone, B. Batlogg, Z. Benes, A. T. Johnson, and J. E. Fischer, *Science* **289**, 1730 (2000).
- [11] G. Granger, D. Taubert, C. E. Young, L. Gaudreau, A. Kam, S. A. Studenikin, P. Zawadzki, D. Harbusch, D. Schuh, W. Wegscheider, Z. R. Wasilewski, A. A. Clerk, S. Ludwig, and A. S. Sachrajda, *Nat. Phys.* **8**, 522 (2012).
- [12] J. Junquera and P. Ghosez, *Nature* **422**, 506 (2003).
- [13] C. Lichtensteiger, P. Zubko, M. Stengel, P. Aguado-Puente, J.-M. Triscone, P. Ghosez, and J. Junquera, in *Oxide Ultrathin Film*. (Wiley-VCH Verlag GmbH & Co. KGaA, 2011), pp. 230–265.
- [14] M. Imada, A. Fujimori, and Y. Tokura, *Rev. Mod. Phys.* **70**, 1039 (1998).
- [15] D. G. Schlom and J. Mannhart, *Nat. Mater.* **10**, 168 (2011).
- [16] a Ohtomo and H. Y. Hwang, *Nature* **427**, 423 (2004).
- [17] S. Thiel, G. Hammerl, A. Schmehl, C. W. Schneider, and J. Mannhart, *Science* **313**, 1942 (2006).
- [18] N. Reyren, S. Thiel, A. D. Caviglia, L. F. Kourkoutis, G. Hammerl, C. Richter, C. W. Schneider, T. Kopp, A.-S. Ruetschi, D. Jaccard, M. Gabby, D. A. Muller, J.-M. Triscone, and J. Mannhart, *Science* **317**, 1196 (2007).
- [19] N. Nakagawa, H. Y. Hwang, and D. A. Muller, *Nat. Mater.* **5**, 204 (2006).
- [20] R. Pentcheva and W. E. Pickett, *Phys. Rev. Lett.* **102**, 107602 (2009).
- [21] M. Stengel, *Phys. Rev. Lett.* **106**, 1 (2011).

- [22] See Supplementary Information at <http://link.aps.org/supplemental/XXXX> for experimental and computational details, as well as additional STEM-EELS data and calculations, which includes Refs. [23-32].
- [23] G. Herranz, F. Sánchez, N. Dix, M. Scigaj, and J. Fontcuberta, *Sci. Rep.* **2**, 3 (2012).
- [24] P. D. Nellist and S. J. Pennycook, *Ultramicroscopy* **78**, 111 (1999).
- [25] Y. K. E Okunishi, I Ishikawa, H Sawada, F Hosokawa, M Hori, E. Okunishi, I. Ishikawa, H. Sawada, F. Hosokawa, M. Hori, Y. Kondo, and Y. K. E Okunishi, I Ishikawa, H Sawada, F Hosokawa, M Hori, *Microsc. Microanal.* **15**, 164 (2009).
- [26] R. Ishikawa, E. Okunishi, H. Sawada, Y. Kondo, F. Hosokawa, and E. Abe, *Nat. Mater.* **10**, 278 (2011).
- [27] R. Ishikawa, A. R. Lupini, F. Oba, S. D. Findlay, N. Shibata, T. Taniguchi, K. Watanabe, H. Hayashi, T. Sakai, I. Tanaka, Y. Ikuhara, and S. J. Pennycook, *Sci. Rep.* **4**, 3778 (2014).
- [28] P. R. Willmott, S. A. Pauli, R. Herger, C. M. Schlepütz, D. Martocchia, B. D. Patterson, B. Delley, R. Clarke, D. Kumah, C. Cionca, and Y. Yacoby, *Phys. Rev. Lett.* **99**, 155502 (2007).
- [29] P. E. Blöchl, *Phys. Rev. B* **50**, 17953 (1994).
- [30] M. Stengel and N. A. Spaldin, *Nature* **443**, 679 (2006).
- [31] M. Stengel, N. A. Spaldin, and D. Vanderbilt, *Nat Phys* **5**, 304 (2009).
- [32] P. Bouvier and J. Kreisel, *J. Phys. Condens. Matter* **14**, 3981 (2002).
- [33] C. L. Jia, S. B. Mi, M. Faley, U. Poppe, J. Schubert, and K. Urban, *Phys. Rev. B* **79**, 81405 (2009).
- [34] C. Cantoni, J. Gazquez, F. Miletto Granozio, M. P. Oxley, M. Varela, A. R. Lupini, S. J. Pennycook, C. Aruta, U. S. di Uccio, P. Perna, and D. Maccariello, *Adv. Mater.* **24**, 3952 (2012).
- [35] A. J. Hatt and N. a. Spaldin, *Phys. Rev. B - Condens. Matter Mater. Phys.* **82**, 1 (2010).
- [36] D. Vanderbilt and W. Zhong, *Ferroelectrics* **206**, 181 (1998).
- [37] C. Cazorla and M. Stengel, *Phys. Rev. B* **92**, 214108 (2015).
- [38] M. Stengel and J. Íñiguez, *Phys. Rev. B* **92**, 235148 (2015).
- [39] N. A. Benedek and C. J. Fennie, *J. Phys. Chem. C* **117**, 13339 (2013).
- [40] J. Hong and D. Vanderbilt, *Phys. Rev. B* **87**, 64104 (2013).
- [41] C. Cen, S. Thiel, G. Hammerl, C. W. Schneider, K. E. Andersen, C. S. Hellberg, J. Mannhart, and J. Levy, *Nat. Mater.* **7**, 298 (2008).
- [42] Y. Xie, C. Bell, Y. Hikita, S. Harashima, and H. Y. Hwang, *Adv. Mater.* **25**, 4735 (2013).
- [43] Z. Liao, M. Huijben, Z. Zhong, N. Gauquelin, S. Macke, R. J. Green, S. Van Aert, J. Verbeeck, G. Van Tendeloo, K. Held, G. A. Sawatzky, G. Koster, and G. Rijnders, *Nat. Mater.* **15**, 425 (2016).
- [44] H. N. Lee, H. M. Christen, M. F. Chisholm, C. M. Rouleau, and D. H. Lowndes, *Nature* **433**, 395 (2005).